PAPER

Check for updates

NiCo$_2$O$_4$ nano-needles as an efficient electro-catalyst for simultaneous water splitting and dye degradation†

Muhammad Bilal,[a] Amna Altaf,[a] Ehmen Bint-E-Khalid,[a] Hafiza Komal Zafar,[a] Nimrah Tahir,[a] Ayman Nafady,[b] Md A. Wahab,[c] Syed Shoaib Ahmad Shah, [ID] [a] Tayyaba Najam [ID] *[d] and Manzar Sohail*[a]

Developing an efficient and non-precious bifunctional catalyst capable of performing water splitting and organic effluent degradation in wastewater is a great challenge. This article reports an efficient bifunctional nanocatalyst based on NiCo$_2$O$_4$, synthesized using a simple one-pot co-precipitation method. We optimized the synthesis conditions by varying the synthesis pH and sodium dodecyl sulfate (SDS) concentrations. The prepared catalyst exhibited excellent catalytic activity for the electrochemical oxygen evolution reaction (OER) and simultaneous methylene blue (MB) dye degradation. Among the catalysts, the catalyst synthesized using 1 g SDS as a surfactant at 100 °C provided the highest current density (658 mA cm^{-2}), lower onset potential (1.34 V *vs.* RHE), lower overpotential (170 mV @ 10 mA cm^{-2}), and smallest Tafel slope (90 mV dec^{-1}) value. Furthermore, the OH$^\cdot$ radicals produced during the OER electrochemically degraded the MB to 90% within 2 hours. The stability test conducted at 20 mA cm^{-2} showed almost negligible loss of the electrochemical response for OER, with 99% retention of the original response. These results strongly suggest that this catalyst is a promising candidate for addressing the challenges of wastewater treatment and energy generation.

1. Introduction

Energy demand has recently increased due to the expanding economy and growing global population. Conventional energy sources are becoming scarce and unable to meet the ever-increasing energy needs, leading to a search for renewable and sustainable energy sources.[1–4] This challenge has necessitated the development of renewable and green energy sources to reduce dependence on fossil fuels.[2,4] One potential solution is molecular hydrogen, which has the highest energy density per mass of any other chemical compound (0.0899 kg N^{-1} m^{-3}) and can serve as a potential means of energy storage.[4–6] Electrochemical water splitting is being investigated as a sustainable and CO$_2$-free method to produce hydrogen.[4,7]

Similarly, organic pollutants such as organic dyes are extensively used in various industries, including paper processing, textiles, leather, agriculture, and medicine. However, their widespread use has resulted in significant water contamination, particularly in areas around the textile industry and chemical laboratories. Various techniques have been employed to address this issue to remove these toxic and colored dyes from wastewater, including electro-coagulation, carbon adsorption, and flocculation.[8–11] Nevertheless, there is still a need to identify new and innovative techniques to tackle water contamination problems cost-effectively. Therefore, researchers worldwide are exploring alternative approaches to remove these toxic dyes from water.

In this context, water splitting is a promising solution for mitigating the depletion of fossil fuels and addressing wastewater treatment issues simultaneously. This process of water splitting involves two half-reactions: hydrogen evolution reaction (HER) and oxygen evolution reaction (OER). However, the OER is kinetically sluggish due to its complicated multistep four-electron transfer process, making it less efficient than the HER.[12–15] Ru and Ir oxides are effective electrocatalysts for reducing the overpotential required for the OER. However, their high cost and limited accessibility necessitate the exploration of alternative electrocatalysts, and long-term stability cannot be ruled out. These alternative options should be abundant in the earth's crust, cost-effective, and have comparable properties to RuO$_2$ and

^{a}Department of Chemistry, School of Natural Sciences, National University of Sciences and Technology, Islamabad, 44000, Pakistan. E-mail: manzar.sohail@sns.nust.edu.pk

^{b}Chemistry Department, College of Science, King Saud University, Riyadh 11451, Saudi Arabia

^{c}Energy and Process Engineering Laboratory, School of Mechanical, Medical and Process Engineering, Faculty of Science, Queensland University of Technology (QUT), 2 George Street, Brisbane, QLD 4000, Australia

^{d}Institute of Chemistry, The Islamia University of Bahawalpur, 63100, Pakistan. E-mail: tayyabanajam@outlook.com

† Electronic supplementary information (ESI) available. See DOI: https://doi.org/10.1039/d3ra03012a

IrO_2.[12,16–18] Among the catalysts, transition metal-based catalysts have gained significant attention due to their advantageous characteristics, such as low cost, stability, eco-friendliness, availability, and facile synthesis.[4,19–23] Mixed metal oxides have demonstrated superior electrocatalytic activity when compared to pure metal or pure metal oxides, as a result of the synergistic effect between two or more metals. This approach has led to the development of electrocatalytic materials such as Cu or Fe-doped mesoporous Co_3O_4 or iron-doped NiO nanoparticles, which exhibit improved catalytic properties and enhanced performance.[24] Among numerous transition metal oxides, nickel cobalt oxide has emerged as one of the most promising catalysts for OER due to its low cost, eco-friendliness, high theoretical capacity, good catalytic activity, considerable electrical conductivity, and good efficiency that is comparable to that of RuO_2 and IrO_2.[24,25] Research on the OER has led to the development of promising electrocatalysts, including $NiCo_2O_4$ nanoflowers,[26] $NiCo_2O_4$ hollow nanospheres,[26,27] $NiCo_2O_4$ nanoflakes,[28] $NiCo_2O_4$ nanowires, $MnCo_2O_4$ nanowires, $ZnCo_2O_4$ nanosheet,[29] NiO,[30] and Co_3O_4. These materials were synthesized with some modifications to achieve various morphologies and structures of mixed nickel–cobalt oxides, demonstrating that morphology plays a crucial role in determining the catalytic activity of nickel cobalt oxide.

This work aims to report on development of a non-precious bifunctional catalyst capable of simultaneously performing oxygen evolution by splitting wastewater and degrading organic pollutant dyes in the water, using the radicals produced during the redox reaction of water splitting. The catalyst, $NiCo_2O_4$, was synthesized using a simple one-pot coprecipitation method, and the synthesis was optimized by adjusting the synthesis temperature and the concentration of the surfactant. Subsequently, the prepared catalyst was tested for its electrochemical performance for the OER reaction of water splitting and its ability to degrade organic pollutants, such as a MB solution, simultaneously. The stability of the catalysts was also tested in the presence of organic dyes in the water during H_2 generation.

2. Experimental details

Nickel chloride hexahydrate, cobalt chloride hexahydrate, sodium dodecyl sulfate (SDS), absolute ethanol, and deionized water were purchased from Sigma-Aldrich company and were used without any further purification. All solutions were prepared using deionized water from a Milli-Q (EQ-7000) direct water purification system (Merck KGaA, Darmstadt 64297, Germany).

2.1. Methodology

The nickel cobalt oxide nanocomposites were synthesized using a simple one-pot facile coprecipitation method. Firstly, separate solutions of nickel chloride hexahydrate and cobalt chloride hexahydrate were prepared. For example, 3 mM of nickel chloride hexahydrate (719 mg) was dissolved in 10 mL of deionized water, and similarly, 3 mM of cobalt chloride hexahydrate (711 mg) was dissolved in 10 mL of deionized water. These solutions were mixed with continuous stirring, and three such mixtures were prepared. Varying amounts of SDS (0.5, 1 and 1.5 g) were added to all the formulations and dissolved. Approximately 10 mL of ethanol was added to each beaker, and the resulting solutions were continuously stirred at 100 °C for 1 hour. The precipitates obtained were centrifuged and separated, washed several times with deionized water and ethanol, and then dried. The precipitates were ground, and the final product was calcined in a chamber furnace at 550 °C for 5 h. To synthesize the nanocomposite, a similar process was followed, except that the reaction temperature was varied, and the amount of SDS was kept constant at 1 g. The reactions were carried out at 50, 100, and 150 °C. A schematic presentation of optimized sample synthesized using 1 g SDS at 100 °C is shown in Fig. 1.

2.2. Fabrication of the electrodes

The electrodes for all $NiCo_2O_4$ nanocomposites were fabricated on $(0.5 \times 1 \text{ cm}^2)$ fluorine-doped tin oxide (FTO) glass slides. Prior to fabrication, the FTO glass slides were well-cleaned by sonicating in ethanol, ultrapure water, and acetone for 15 minutes each. $NiCo_2O_4$ nanocomposite slurries were then prepared by mixing 1 mg of each material with 2 mL of ethanol, and the resulting ink was ultrasonicated for 30 minutes to ensure homogenous dispersion. Subsequently, 100 μL of the ink was drop-cast onto the conducting side of the FTO glass slides. After deposition, the FTOs were dried on a hot plate at 60 °C.
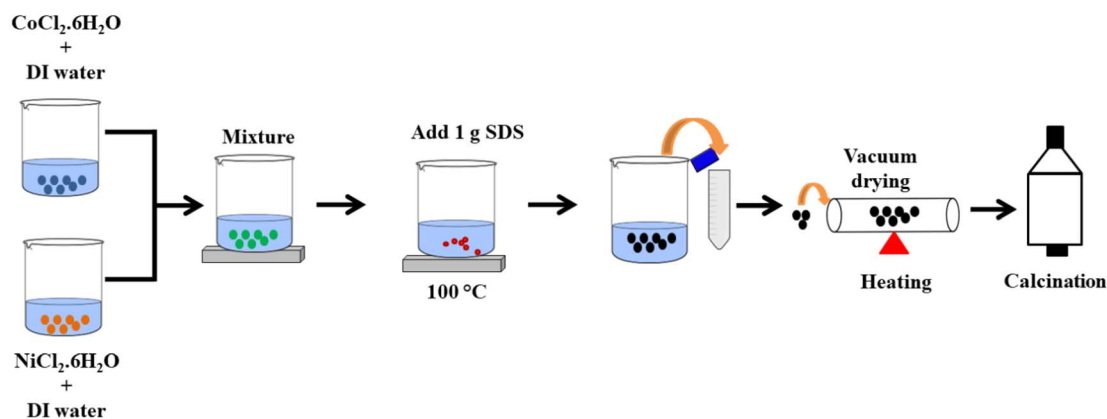

Fig. 1 Schematic illustration of the optimized sample.

2.3. Electrochemical degradation of methylene blue (MB)

To carry out the electrochemical degradation of MB, a dye solution of 10 parts per million (ppm) was prepared and its λ_{max} was measured as 663 nm using a UV-Vis spectrophotometer. The prepared dye solution was introduced into the electrochemical cell at 15 minute intervals while being continuously stirred. The absorbance of the solution was monitored every 15 minutes using the same procedure for each interval.

2.4. Structural characterizations

The powder X-ray diffraction (p-XRD) patterns for all the samples were record using the Bourevestnik Dron-8 diffractometer (St. Petersburg 190900, Russia), equipped with Cu-Kα radiation ($\lambda = 1.5406$ Å) at 20 kV and 40 mA. To study the structural and elemental composition, energy-dispersive X-ray spectroscopy (EDX), scanning electron microscopy (SEM), and elemental mapping were performed using a Nova Nano-SEM 450 electron microscope (Lincoln, NE 68588, United States). For electrochemical performance evaluation, various electrochemical studies such as linear sweep voltammetry (LSV), cyclic voltammetry (CV), chronopotentiometry (CP), and electrochemical impedance spectroscopy (EIS) were conducted using Gamry Interface 1000 electrochemical workstation (Corrtest Instrument, Model CS350M) with a conventional three-electrode system. Nitrogen adsorption–desorption experiments were conducted using a Micrometrics Gemini VII2390t instrument to determine the specific surface area (SSA) of the sample. The SSA was evaluated employing the Brunauer–Emmett–Teller (BET) method, while the Barrett–Joyner–Halenda (BJH) method was applied to obtain pore size distribution curves. Transmission electron microscopy (TEM) was utilized to conduct a detailed investigation of the sample's atomic structure and composition. By employing FEI Talos F200X TEM, high-resolution image and valuable information about the sample's structural properties were obtained. TEM utilizes a focused electron beam to create images of the material's internal structure at 5 nm. The resulting electron scattering and diffraction patterns provide insights into the crystal structure, defects, and compositional variations within the material, offering a comprehensive understanding of its atomic arrangement.

3. Results and discussions

The p-XRD patterns of the prepared thin films at different reaction temperatures are shown in Fig. 2(a). The obtained p-XRD patterns of $NiCo_2O_4$ exhibit well-defined diffraction peaks, indicating the crystalline nature of the nano-composites.[31] When synthesized at 50 °C, sharp peaks were observed, which contrasted with higher temperatures. As the temperature increased to 100 °C and 150 °C, the peak size becomes broadened, indicating that higher synthesis temperatures resulted in smaller crystallites forming.[32] The observed peaks at 2θ 21°, 33.8°, 37°, 43°, and 65.5° corresponded to hkl values of (111), (220), (311), (400), and (440), respectively, and matched well with the p-XRD pattern of $NiCo_2O_4$.[33] Fig. 2(b) shows the p-XRD patterns of the as-prepared samples at varying concentrations of SDS, revealing that an increase in SDS concentration leads to broader peaks, indicating a reduction in the crystallite size. OER reaction can cause $NiCo_2O_4$ thin film to oxidize into NiO and decompose existing phases, detected through XRD analysis. The p-XRD of the respective oxides before and after electrochemistry are shown in Fig. S1† to reveal the stability of the catalyst.

The surface morphologies of catalyst samples prepared with different reaction temperatures and SDS concentrations were analyzed using scanning electron microscopy (SEM). SEM images revealed that the particle size of $NiCo_2O_4$ (50 °C) was larger at lower reaction temperatures, while an increase in temperature to 100 °C with 1 g SDS concentration resulted in increased porosity of $NiCo_2O_4$. Further temperature increases in $NiCo_2O_4$ (150 °C) led to the agglomeration of nanoparticles. Fig. 3(a) displays the well-defined petals and needle-like morphologies of $NiCo_2O_4$ (100 °C) with 1 g SDS concentration, which are beneficial in creating active sites during the reactions. In contrast, $NiCo_2O_4$ (0.5 g SDS) resulted in bigger and agglomerated particles. SDS acted as a dispersing agent,
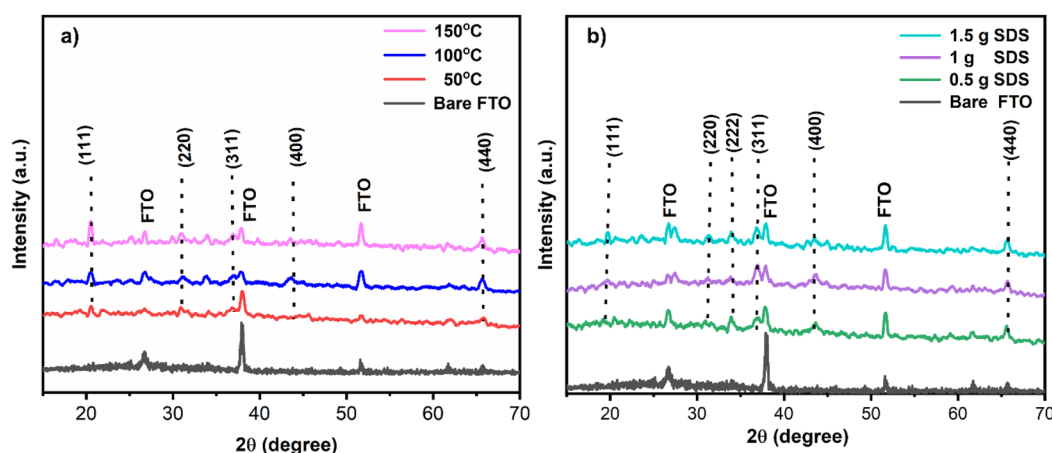

Fig. 2   p-XRD graph of $NiCo_2O_4$ nanostructures synthesized at (a) different reaction temperatures (b) different SDS concentrations.
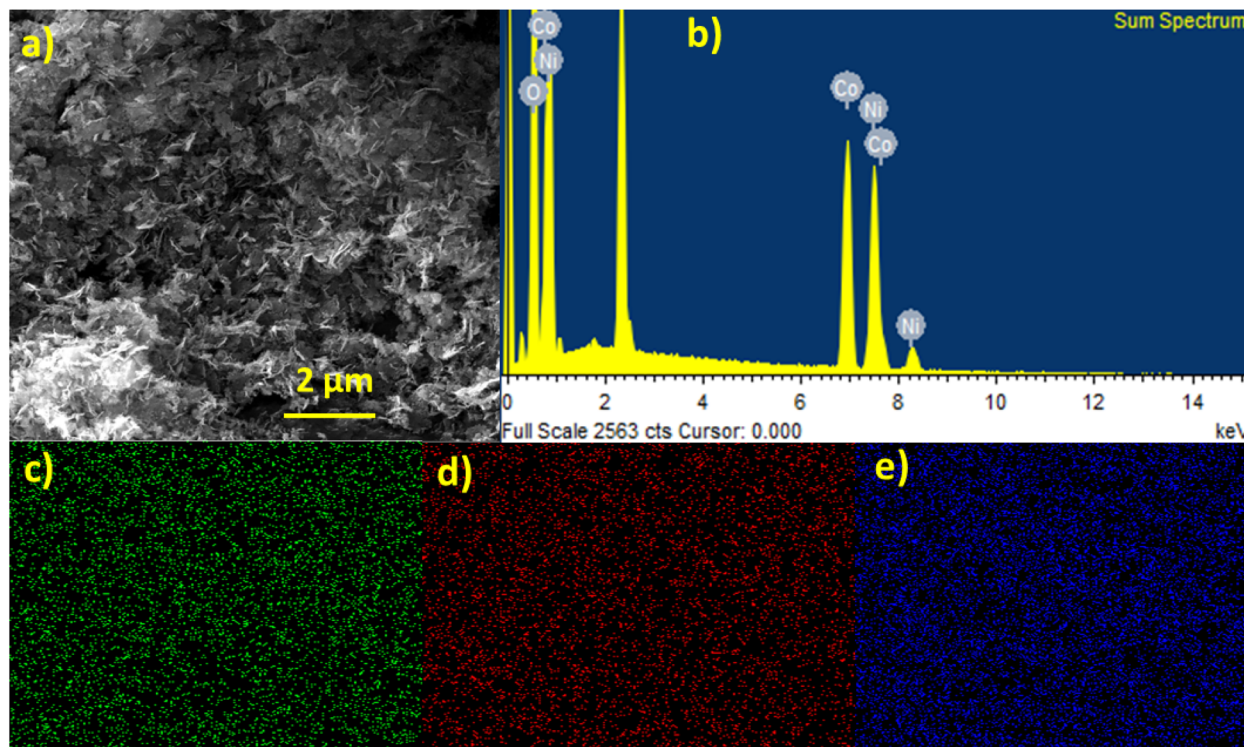
Fig. 3 $NiCo_2O_4$ nanostructures synthesized at 100 °C with 1 g SDS (a) SEM images (b–e) EDX and elemental mapping.

preventing the agglomeration of the nanoparticles, and enhancing their contact with the electrolyte solution. At 0.5 g of SDS, the amount of surfactant may be insufficient to effectively stabilize and disperse the nanoparticles, leading to the formation of larger and less uniform nanoparticles or agglomerates. Whereas 1 g of SDS may be the optimized concentration for uniform dispersion and formation of well-defined petals and needle-like morphologies with desired properties.[34,35] SEM images of $NiCo_2O_4$ synthesized at different temperatures and SDS concentrations are also shown in Fig. S2 (ESI†). EDX (Energy Dispersive X-ray) analysis was employed to provide information about the elemental composition of the samples, including the type and concentration of elements present. Fig. 3(b) shows the EDX, indicating the presence of Co, Ni, and oxide. Elemental mapping of $NiCo_2O_4$ (100 °C, 1 g SDS) is also displayed in Fig. 3(c)–(e), indicating the uniform distribution of Ni, Co, and O throughout the scanned area, confirming the homogeneous formation of the $NiCo_2O_4$ nanocomposites.

The surface characteristics of $NiCo_2O_4$ nanostructures synthesized at 100 °C with 1 g SDS were assessed through N_2 adsorption–desorption isotherms, revealing a type-IV isotherm associated with well-defined pore structures and mesoporous materials as shown in Fig. 4(a). The determined BET SSA for $NiCo_2O_4$ nanostructures synthesized at 100 °C with 1 g SDS was determined to be 344.94 m^2 g^{-1}, a substantial value attributed to its distinct petals and needle-like morphology. This large SSA suggests the presence of abundant active sites and high porosity, rendering $NiCo_2O_4$ highly advantageous for electrochemical water splitting and MB dye removal. The analysis

further revealed the existence of mesopores with a characteristic diameter of 7.7 nm as shown in Fig. 4(b), reinforcing $NiCo_2O_4$'s porous nature, which facilitates efficient transport and migration of ions during electrocatalytic reaction.

The TEM image presented in Fig. 4(d) was utilized to examine the lattice fringes of the $NiCo_2O_4$ nanocomposite synthesized at 100 °C with 1 g SDS. The observed lattice spacing of 0.39 nm in Fig. 4(c) corresponds to the (111) plane, while the lattice spacing of 0.34 nm in Fig. 4(e) corresponds to the (220) plane of $NiCo_2O_4$. These lattice spacings provide valuable insights into the crystallographic orientation and arrangement of the nanocomposite material. By analyzing the lattice fringes in TEM images, we can gain a deeper understanding of the structural characteristics and properties of $NiCo_2O_4$ nanocomposite synthesized at 100 °C with 1 g SDS nanocomposite.

3.1. Electrochemical studies

To evaluate the electrochemical catalytic activity of the $NiCo_2O_4$ nanocomposites synthesized under different reaction temperatures and SDS concentrations for the OER, various electrochemical tests, such as CV, LSV, and chronoamperometry were conducted and compared with other synthesized catalysts. The electrochemical measurements were carried out in a 1 M KOH aqueous solution (pH = 14). LSV was performed using a potential window of 1.3 to 1.75 V (vs. RHE) at a scan rate of 5 mV s^{-1}. The CV curves for all $NiCo_2O_4$ nanocomposites synthesized under different reaction temperatures and SDS concentrations are displayed in Fig. S3.† To determine the overpotentials resulting from strong oxidation peaks observed in the forward
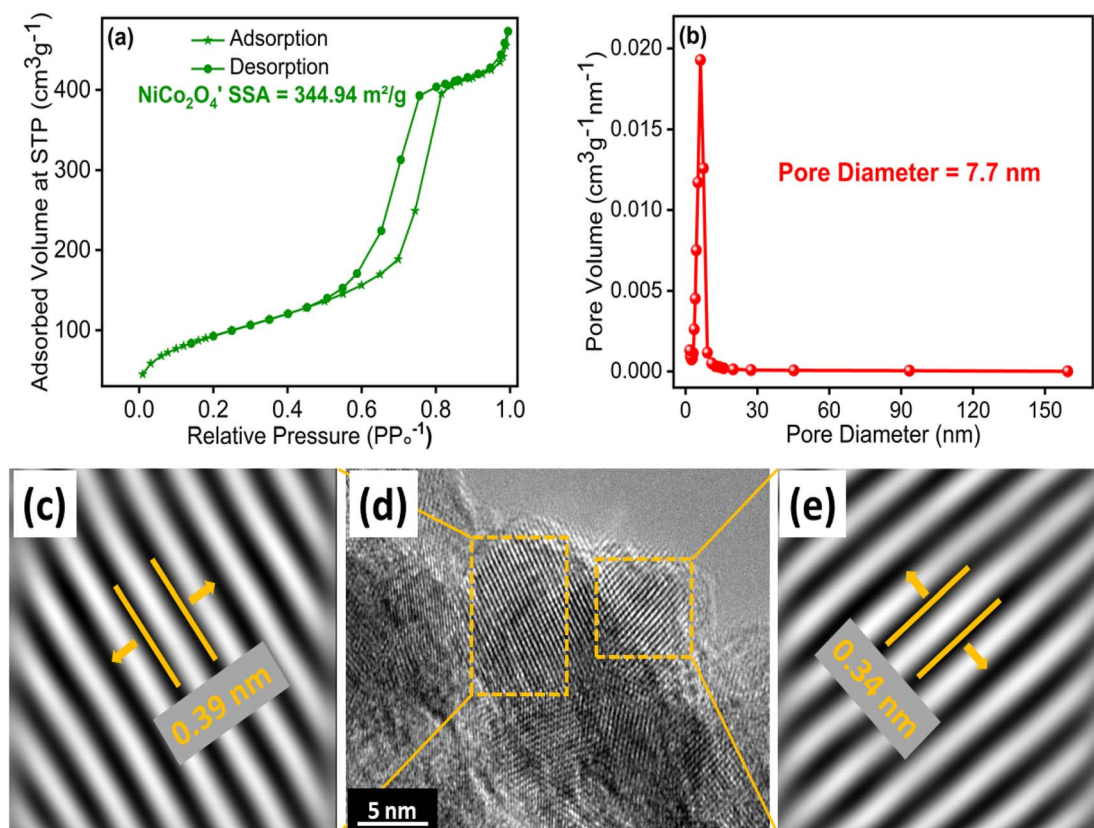
Fig. 4 $NiCo_2O_4$ nanostructures synthesized at 100 °C with 1 g SDS (a) N_2 adsorption–desorption isotherms, (b) pore size distribution, (c–e) HR-TEM with inversed fast Fourier transform (IFFT) images.

CV scans for the $NiCo_2O_4$ nanocomposite, reverse CV scans were employed. Furthermore, all cyclic voltammetry (CV) curves demonstrate distorted rectangular shapes at lower scan rates, indicating that the materials can store charges on their surface and at the electrode–electrolyte interface, confirming the presence of an electrical double-layer capacitance. Despite the increase in current density with increasing scan rate, the rectangular shape of the CV curve remains consistent. These results demonstrate that the $NiCo_2O_4$ catalyst synthesized at a temperature of 100 °C, utilizing 1 g concentration of SDS in the reaction mixture, exhibited the highest current densities and reduced overpotentials for the OER compared to those synthesized at temperatures of 50 °C and 150 °C. $NiCo_2O_4$ catalyst (100 °C) showed onset potential of 1.34 V $vs.$ RHE with overpotential of 170 mV, 370 mV and 400 mV at current densities of 10, 50 and 100 mA cm^{-2}, respectively, which is lower than that of $NiCo_2O_4$ catalyst (50 °C) and $NiCo_2O_4$ catalyst (150 °C) as shown in Fig. 5(a). This observation can be attributed to the highly porous nature and greater surface area of the former catalyst, which is likely to have facilitated the OER, as confirmed by SEM images.

It is noteworthy that the utilization of 1 g SDS during the synthesis of $NiCo_2O_4$ nanocomposites at a temperature of 100 °C resulted in superior OER performance when compared to those synthesized using SDS concentrations of 0.5 g and 1.5 g. The highest current density of 658 mA cm^{-2} and an overpotential of 170 mV, 370 mV and 400 mV at current densities of

10, 50 and 100 mA cm^{-2}, respectively were achieved with $NiCo_2O_4$ catalyst (1 g SDS) as shown in Fig. 5(b). The overpotential calculations at 10, 50 and 100 mA, synthesized by using 1 g SDS and 100 °C temperature is demonstrated in Fig. S5.† These results were superior to those obtained with $NiCo_2O_4$ catalysts synthesized using 0.5 g and 1.5 g SDS concentrations. This outcome can be attributed to the highly porous nature of the material, as observed in SEM images, and the smaller particle sizes apparent in p-XRD peaks.

To evaluate the Tafel plots of all the as-prepared samples, the linear regions were fitted into the Tafel equation ($\eta = b \log J + a$),[36] where b represents the Tafel slope. Tafel plots provide insights into reaction mechanisms as well as electrode properties, with a small Tafel slope value indicating well-balanced kinetic during electrocatalysis.[37] Among the employed synthesis temperatures, $NiCo_2O_4$ synthesized at 100 °C exhibited a much lower Tafel slope value of 90 mV dec^{-1} compared to $NiCo_2O_4$ synthesized at 50 °C and 150 °C, having Tafel values of 99 mV dec^{-1} and 94 mV dec^{-1} respectively, as shown in Fig. 5(c). Similarly, for different SDS concentrations, $NiCo_2O_4$ synthesized with 1 g of SDS exhibited a lower Tafel slope value, 111 mV dec^{-1} than that of $NiCo_2O_4$ synthesized with 0.5 g of SDS and $NiCo_2O_4$ 1.5 g of SDS, having Tafel values of 245 mV dec^{-1} and 235 mV dec^{-1}, respectively, as shown in Fig. 5(d). An ideal catalyst for achieving optimal OER performance should exhibit low overpotential and Tafel slope values, while also
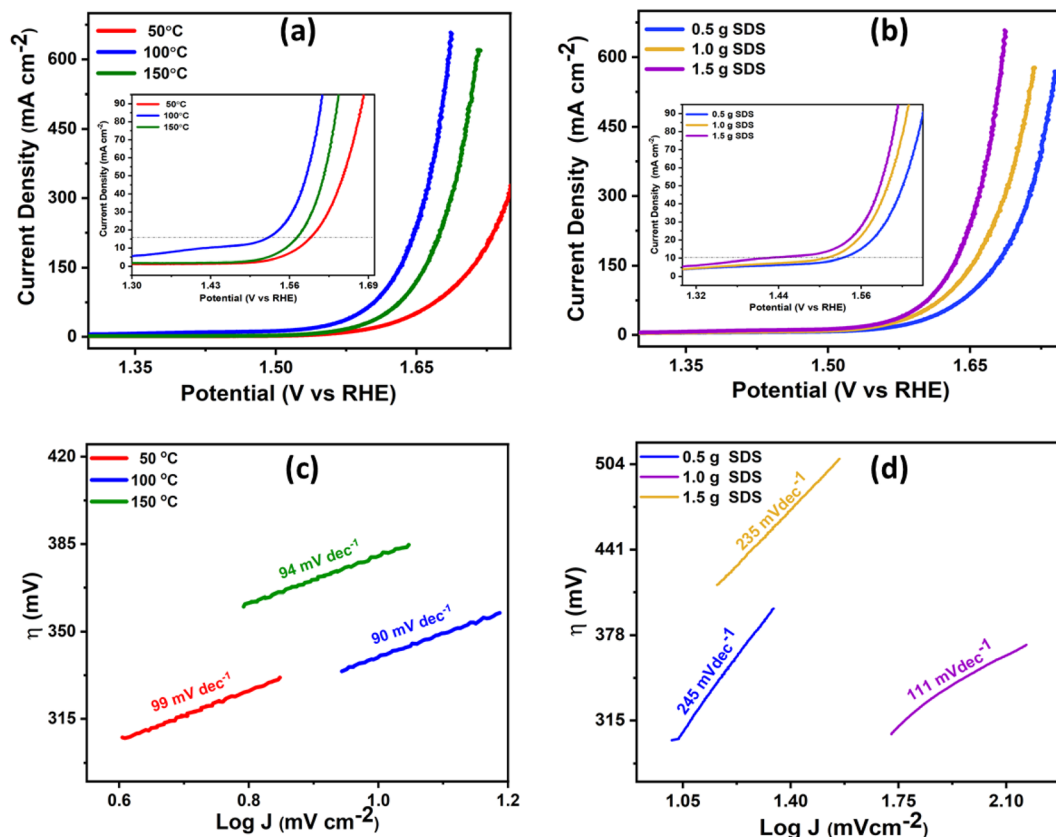
Fig. 5 Linear sweep voltammetry comparison of $NiCo_2O_4$ at different (a) temperatures, (b) SDS concentrations with insets showing onset and overpotential values and Tafel plot of $NiCo_2O_4$ synthesized at different (c) temperature, (d) SDS concentrations.

demonstrating high current density. After considering all relevant factors studied here, the most effective catalyst is the one synthesized at a temperature of 100 °C with 1 g of SDS, $NiCo_2O_4$ (100 °C, 1 g SDS). At this optimum condition, $NiCo_2O_4$ nanoparticles result in well-defined petals and needle-like morphologies, providing larger surface area and active sites. Therefore, it will result in enhanced electrocatalytic activity and stability during OER, leading to improved electrochemical performance.

Furthermore, ESI Table 1† provides the OER activities of various electrocatalysts possessing different morphologies, in addition to the findings of this study. This table clearly demonstrates that our catalyst, $NiCo_2O_4$ (petals and needle-like morphology) synthesized with 1 g of SDS at 100 °C, exhibited the lowest overpotential value of 170 mV @ 10 mA cm^{-2} as compared to different morphologies of $NiCo_2O_4$, NiO, Co_3O_4, $MnCo_2O_4$, and $ZnCo_2O_4$. Other $NiCo_2O_4$ morphologies such as nanoflowers, hollow nanospheres, nanoflakes and nanowires show overpotential values of 383, 428, 360 and 271 mV @ 10 mA cm^{-2} respectively, whereas NiO, Co_3O_4, $MnCo_2O_4$, and $ZnCo_2O_4$ give overpotential values of 470, 498, 289 and 340 mV @ 10 mA cm^{-2} respectively. This comparison further confirms the exceptional catalytic performance of our catalyst in electrochemical water splitting.

Electrochemical impedance spectroscopy (EIS) was conducted to investigate the reaction kinetics of the prepared

electrocatalysts in this study.[38] This technique measures the charge transfer resistance R_{ct} and relates it to electrocatalytic activity. EIS measurements were performed under a constant potential of 300 mV by using 1.0 M KOH as an electrolyte. To minimize variations in solution resistance, freshly prepared electrolyte was utilized for each electrocatalytic experiment. The Nyquist EIS plots of all samples, synthesized at varying temperatures and surfactant content, are presented in Fig. 6(a) and (b). To fit the EIS data, a circuit equivalent circuit was designed. This circuit comprised two resistors and one capacitor element, in addition to Yo13, a14 and Yo15, b16 these are the constant phase elements,[12] and is illustrated in Fig. S4.† The circuit facilitated calculation of R_{ct} and R_s. R_{ct}, which is the interfacial resistance between the material and the electrolyte, determines the kinetics of charge transfer in the oxygen evolution reaction (OER), while R_s represents the solution resistance.[39]

When investigating the effects of temperature, it was observed that $NiCo_2O_4$ synthesized at 100 °C exhibited superior kinetics and the lowest charge transfer resistance of 1.3 Ω, compared to $NiCo_2O_4$ catalysts synthesized at 50 °C and at 150 °C, which had the charge transfer resistance values of 4.8 Ω and 2.7 Ω, respectively, as shown in Fig. 6(a). This result is consistent with the LSV results. For SDS various concentration studies, $NiCo_2O_4$ (synthesized with 1 g of SDS) displayed the most favorable kinetics and the lowest charge transfer resistance of
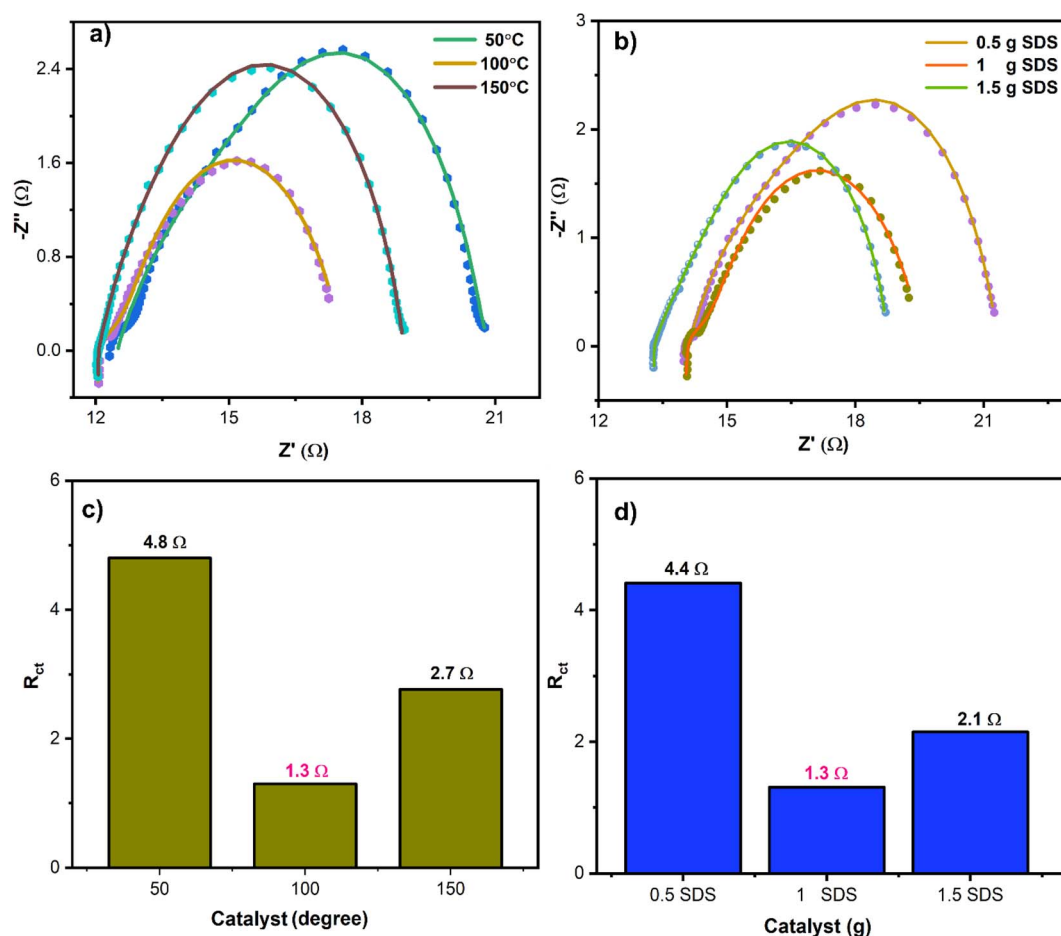
Fig. 6 Electrochemical impedance spectroscopy of $NiCo_2O_4$ at (a) different temperature, (b) different SDS amounts fitted with the designed circuit and bar graph of resistance of $NiCo_2O_4$ at (c) different temperature, (d) different SDS amount.

1.3 Ω compared to $NiCo_2O_4$ catalyst synthesized with 0.5 g of SDS and 1.5 g of SDS, which had the charge transfer resistance values of 4.4 Ω and 2.1 Ω, respectively, as depicted in Fig. 6(b). To provide a deeper understanding of the variations in charge transfer resistance across all synthesized catalysts, bar graphs of R_{ct} values are presented in Fig. 6(c) and (d). The results of the EIS studies indicate that the optimal material is $NiCo_2O_4$ (100 °C, 1 g SDS), which demonstrates the lowest charge transfer resistance of 1.3 Ω and higher favorable kinetics than the other $NiCo_2O_4$ catalysts. These findings align well with the results of CV, LSV, SEM, and p-XRD.

The results of the study indicate that the findings are in excellent agreement with the polarization curves obtained from the LSV and CV analyses. Importantly, the $NiCo_2O_4$ catalyst synthesized at 100 °C with 1 g of SDS exhibited the highest current density and minimum over-potential, which can be attributed to its improved porosity and increased electrochemical surface area, as well as its comparatively lower Tafel slope and smaller EIS value. The higher electrocatalytic activity for OER can be attributed to the phase transition of nickel hydroxide (NiOOH) and Cobalt hydroxide (CoOOH), whereby the oxidation of CoOOH to CoO_2 leads to a more efficient OER process. Additionally, at the same potential, Ni is also oxidized

to Ni^{3+}. Therefore, the overall mechanism for the reaction involves the oxidation of CoOOH to CoO_2, leading to increased OER activity, while also oxidizing Ni to Ni^{3+}.[40] The process proceeds as follows:

$$NiCoO_2 + 2OH^- \rightarrow NiOOH + CoOOH + 2e^-$$
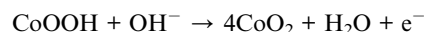
$$CoOOH + OH^- \rightarrow 4CoO_2 + H_2O + e^-$$

Fig. 7(a) and (b) show the electrochemical surface area (ECSA) of the optimized catalyst. ECSA measures the active surface area of an electrocatalyst participating in electrochemical reactions, an essential parameter for assessing the performance of electrocatalysts in various electrochemical applications. The ECSA of $NiCo_2O_4$ catalyst synthesized at 100 °C with 1 g of SDS is determined to be 1385 cm² derived from the C_{dl} value shown in Fig. 7(a). ECSA of other catalysts has also been investigated. The catalyst synthesized by using 0.5 g and 1.5 g SDS exhibit ECSA of 24.5 cm² and 590 cm² respectively, as shown in Fig. S6(a) and (b).† Similarly, samples synthesized at different temperatures i.e. 50 °C, 100 °C exhibits the ECSA of 300 cm² and 612 cm² respectively, as shown in Fig. S6(c) and
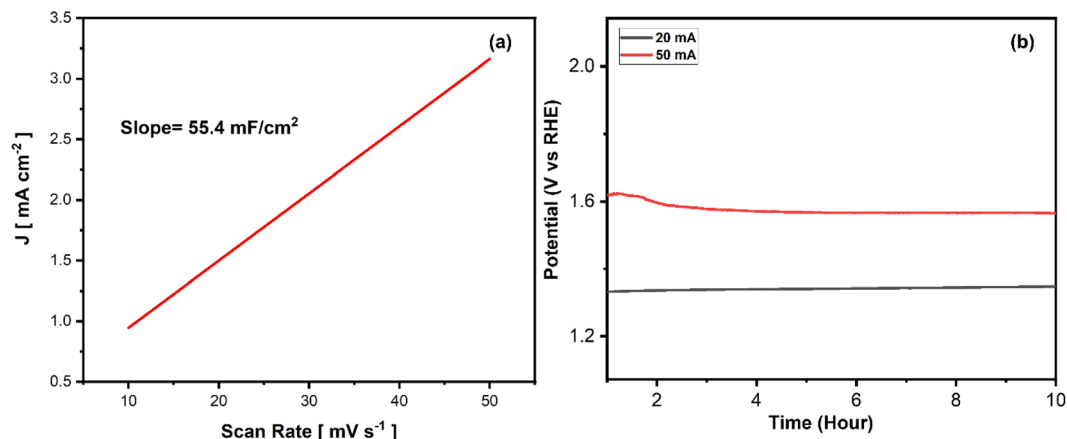
Fig. 7 (a) Electrochemically active surface area and (b) stability of NiCo$_2$O$_4$ synthesized at 100 °C temperature and 1 g SDS concentration.

(d).† This highest ECSA (1385 cm^2) of the optimized sample (1 g SDS, 100 °C) corresponds to a greater number of active sites available for electrochemical reactions, leading to improved electrocatalytic activity. For industrial application and commercialization of the catalyst, the long-term stability of the catalysts is of great importance. To assess the durability of the electrocatalysts, chronoamperometric scans at different voltage and current values are employed. The present study investigates the long-term catalytic performance of the thin film of best NiCo$_2$O$_4$ (100 °C, 1 g SDS) catalyst for OER under electrochemical conditions employed in this study, demonstrating excellent stability. The thin films exhibited sustained potential values for OER under harsh oxidative environments, as depicted in Fig. 7(b), at constant current densities of 20 mA cm^{-2} and 50 mA cm^{-2}, respectively. The stability test conducted at 20 mA cm^{-2} showed almost zero degradation, with 99% catalyst retention, again substantiating the outstanding stability of the catalyst used. However, in the case of 50 mA cm^{-2}, a decrease in overpotential was observed which might be due to the increase in the porosity and further oxidation of cobalt and nickel at the surface of the electrode, which can provide additional facets for the OER. This test was conducted for a prolonged duration of 10 h.

3.2. Electrocatalytic MB degradation

MB is a toxic and water-soluble organic pollutant that has been widely studied. It is commonly present in the wastewater of various industrial processes, posing a significant risk to human health. Therefore, the removal of MB from contaminated water sources is of paramount importance.[23] The NiCo$_2$O$_4$ catalyst synthesized at 100 °C with 1 g of SDS was utilized to simultaneously generate oxygen and effectively degrade MB. The results indicate 90% degradation of MB within a 120 minute timeframe, as shown in Fig. 8(a). The percentage degradation of MB was calculated using the formula given below:

$$\% \ D = A_0 - A_t/A_0 \times 100$$

where, A_t is the absorbance at 60 min and A_0 represents the absorbance at time 0. By using this formula % degradation was found to be 90% as shown in Fig. 8(b).

3.3. Proposed mechanism of electrocatalytic MB degradation along with OER

The mechanism of electrocatalytic degradation of MB along OER involves using an electrode (NiCo$_2$O$_4$ (synthesized at 100 °C with

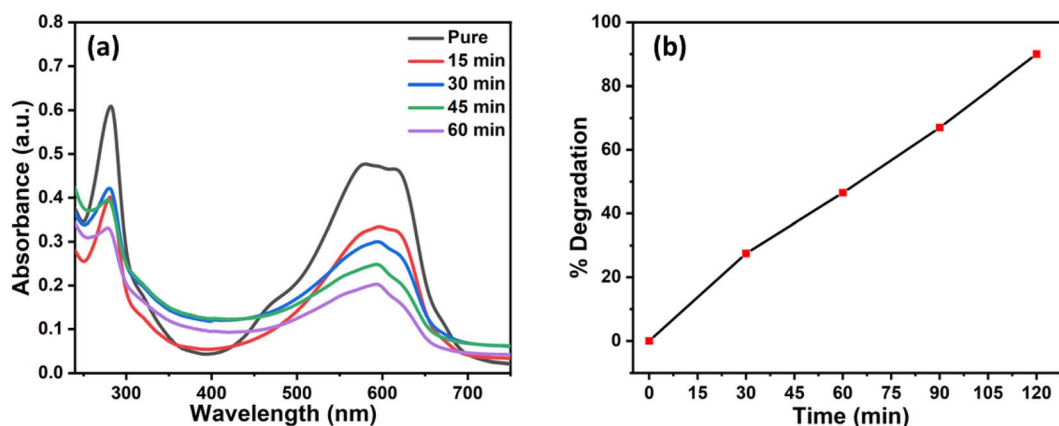Fig. 8 (a) Electrochemical degradation and (b) % degradation of methylene blue by NiCo$_2$O$_4$ (100 °C, 1 g SDS).

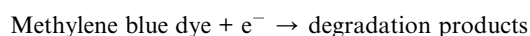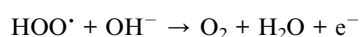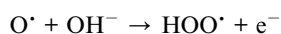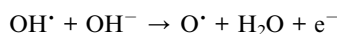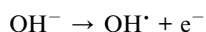1 g of SDS)/FTO) as a catalyst to facilitate both processes simultaneously. The OER process involves oxidizing water molecules at the anode, which generate oxygen gas and protons. The protons and electrons from the cathode then combine to form water again. This process occurs at the same time as the MB degradation reaction, where the electrode produces reactive oxygen species (ROS) such as hydroxyl radicals (OH$^{\cdot}$) that react with MB molecules to break them down into smaller, less harmful compounds. The ROS attack the MB molecules by abstracting hydrogen atoms or electrons from them, leading to the formation of intermediate species that undergo further reactions, eventually resulting in carbon dioxide, water, and other byproducts. The OER process provides the electrons needed for the degradation reaction and also prevents the accumulation of hydrogen gas, which can impede the degradation process. Overall, this approach is promising for treating dye-contaminated wastewater because it is ecofriendly and energy-efficient, achieving high removal rates while producing minimal byproducts.[41]

A possible mechanism of OER along with MB degradation is as follows:

The mechanism of OER under alkaline conditions is as follows:

$$4OH^- \rightarrow O_2 + 4H^+ + 4e^-$$
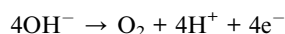
This reaction proceeds in the following four steps.

$$OH^- \rightarrow OH^{\cdot} + e^-$$

$$OH^{\cdot} + OH^- \rightarrow O^{\cdot} + H_2O + e^-$$

$$O^{\cdot} + OH^- \rightarrow HOO^{\cdot} + e^-$$

$$HOO^{\cdot} + OH^- \rightarrow O_2 + H_2O + e^-$$

$$\text{Methylene blue dye} + OH^{\cdot} \rightarrow CO_2 + H_2O \text{ (dye intermediates)}$$

$$\text{Methylene blue dye} + e^- \rightarrow \text{degradation products}$$
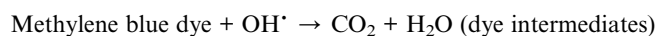
Simultaneous conducting the electrocatalytic degradation of MB and the OER has several advantages over conducting them separately. When both reactions occur together, they can synergistically enhance each other, such that OER process provides the electrons needed for the MB degradation reaction, while the degradation reaction consumes the OH$^{\cdot}$ generated during OER. This synergy leads to improved efficiency and selectivity of the overall process. Conducting both reactions together reduce the energy consumption required to drive each reaction separately. It also enhances the reaction kinetics and reduces the reaction time required to achieve complete MB degradation. This is because the electrocatalytic reaction provides a more efficient and controlled mechanism for the degradation of MB molecules. Combining both reactions together reduce the overall cost of the process by minimizing the number of components and the complexity of the system required to achieve complete MB degradation. This method could solve two daunting issues of energy crisis and wastewater treatment simultaneously. The comprehensive degradation of a significant number of dyes can be accomplished while generating a substantial amount of energy. Therefore, this method offers a promising solution to both challenges and make it a promising approach for treating the dye-contaminated wastewater.

4. Conclusion

In conclusion, this study has successfully synthesized NiCo$_2$O$_4$ using a straightforward one-pot facile coprecipitation method and comprehensively characterized it by p-XRD, SEM and EDX. The electrocatalytic water splitting and MB degradation performances of the prepared NiCo$_2$O$_4$ were investigated, and the results showed that NiCo$_2$O$_4$ (100 °C, 1 g SDS) exhibited exceptional catalytic activity. Specifically, this catalyst demonstrated a current density of 658 mA cm^{-2}, lower onset potential of 1.34 V vs. RHE and the least overpotential of 170 mV, 370 mV and 400 mV at current densities of 10, 50 and 100 mA cm^{-2}, respectively, and remained stable for 10 hours. Furthermore, the as-synthesized catalyst effectively degraded MB electrochemically within a short period of 60 min. Overall, this study highlights the potential of synthesizing highly efficient bifunctional catalysts capable of simultaneously generating energy and treating wastewater.

Author contributions

Muhammad Bilal: investigation, experiments. Amna Altaf: writing original draft, formal analysis, data curation. Ehmen Bint-E-Khalid: writing original draft. Ayman Nafady: writing – reviewing, funding acquisition. Md Abdul Wahab: methodology, conceptualization, writing – reviewing. Nimra Tahir: experiments, data curation. Syed Shoaib Ahmad Shah: conceptualization, review & editing. Tayyaba Najam: conceptualization, review & editing. Manzar Sohail: conceptualization, writing – review & editing, supervision, funding acquisition.

Conflicts of interest

The authors declare that they have no known competing financial interests or personal relationships that could have appeared to influence the work reported in this paper.

Acknowledgements

References

1 P. V. Kamat, Meeting the Clean Energy Demand: Nanostructure Architectures for Solar Energy Conversion, *J. Phys. Chem. C*, 2007, **111**, 2834–2860.

View Article Online

RSC Advances

Paper

Open Access Article. Published on 07 August 2023. Downloaded on 12/9/2025 10:32:16 AM. This article is licensed under a Creative Commons Attribution-NonCommercial 3.0 Unported Licence.

2 J. Zhao, *et al.*, Engineering the Surface Metal Active Sites of Nickel Cobalt Oxide Nanoplates toward Enhanced Oxygen Electrocatalysis for Zn-Air Battery, *ACS Appl. Mater. Interfaces*, 2019, **11**(5), 4915–4921.

3 S. Peng, *et al.*, Necklace-like Multishelled Hollow Spinel Oxides with Oxygen Vacancies for Efficient Water Electrolysis, *J. Am. Chem. Soc.*, 2018, **140**(42), 13644–13653.

4 K. Zhang and R. Zou, Advanced Transition Metal-Based OER Electrocatalysts: Current Status, Opportunities, and Challenges, *Small*, 2021, **17**(37), e2100129.

5 S. Sharifian, *et al.*, Dynamic Simulation of Hydrogen Generation from Renewable Energy Sources, *Chem. Eng. Trans.*, 2015, **45**, 409–414.

6 W. Zeb, Enhanced photoelectrochemical performance of P-doped g-C_3N_4/$Zn_{0.5}Cd_{0.5}$S heterojunction photocathode for water splitting, *J. Saudi Chem. Soc.*, 2022, **26**(6), 101542.

7 S. Cobo, *et al.*, A Janus cobalt-based catalytic material for electro-splitting of water, *Nat. Mater.*, 2012, **11**(9), 802–807.

8 H. Wang, Comparison of dye degradation efficiency using ZnO powders with various size scales, *J. Hazard. Mater.*, 2007, **141**(3), 645–652.

9 A. Alinsafi, Electro-coagulation of reactive textile dyes and textile wastewater, *Chem. Eng. Process.: Process Intensif.*, 2005, **44**(4), 461–470.

10 S. Papić, Removal of some reactive dyes from synthetic wastewater by combined Al (III) coagulation/carbon adsorption process, *Dyes Pigm.*, 2004, **62**(3), 291–298.

11 C. Allegre, Coagulation–flocculation–decantation of dye house effluents: concentrated effluents, *J. Hazard. Mater.*, 2004, **116**(1–2), 57–64.

12 M. Bilal, *et al.*, Crystalline and porous CoSe dendrimeric architectures for efficient oxygen evolution reaction, *Fuel*, 2022, **323**, 124324.

13 F. Lyu, *et al.*, Self-Templated Fabrication of CoO–MoO_2 Nanocages for Enhanced Oxygen Evolution, *Adv. Funct. Mater.*, 2017, **27**(34), 1702324.

14 V. Tripkovic, H. A. Hansen and T. Vegge, From 3D to 2D Co and Ni Oxyhydroxide Catalysts: Elucidation of the Active Site and Influence of Doping on the Oxygen Evolution Activity, *ACS Catal.*, 2017, **7**(12), 8558–8571.

15 S. Ramakrishnan, *et al.*, Nitrogen-doped graphene encapsulated FeCoMoS nanoparticles as advanced trifunctional catalyst for water splitting devices and zinc–air batteries, *Appl. Catal., B*, 2020, **279**, 119381.

16 Y. Lee, *et al.*, Synthesis and Activities of Rutile IrO_2 and RuO_2 Nanoparticles for Oxygen Evolution in Acid and Alkaline Solutions, *J. Phys. Chem. Lett.*, 2012, **3**(3), 399–404.

17 H. Xu, *et al.*, Porous Microrod Arrays Constructed by Carbon-Confined NiCo@NiCoO$_2$ Core@Shell Nanoparticles as Efficient Electrocatalysts for Oxygen Evolution, *Adv. Mater.*, 2018, **30**(21), e1705442.

18 J. W. Zhao, *et al.*, Boosting Lattice Oxygen Oxidation of Perovskite to Efficiently Catalyze Oxygen Evolution Reaction by FeOOH Decoration, *Research*, 2020, **2020**, 6961578.

19 F. Lyu, *et al.*, Noble-Metal-Free Electrocatalysts for Oxygen Evolution, *Small*, 2019, **15**(1), e1804201.

20 L. Lv, *et al.*, Electronic coupling regulation in yolk-shell nanostructured nickel-cobalt diselenides with octahedral coordination for boosted oxygen evolution reaction, *Int. J. Hydrogen Energy*, 2021, **46**(56), 28387–28396.

21 Y. Yan, *et al.*, A review on noble-metal-free bifunctional heterogeneous catalysts for overall electrochemical water splitting, *J. Mater. Chem. A*, 2016, **4**(45), 17587–17603.

22 M. Plevová, J. Hnát and K. Bouzek, Electrocatalysts for the oxygen evolution reaction in alkaline and neutral media. A comparative review, *J. Power Sources*, 2021, **507**, 230072.

23 Y. F. Jatoi, M. Fiaz and M. Athar, Synthesis of efficient TiO_2/Al_2O_3@Cu (BDC) composite for water splitting and photodegradation of methylene blue, *J. Aust. Ceram. Soc.*, 2021, **57**(2), 489–496.

24 X. Deng, *et al.*, Iron-Induced Activation of Ordered Mesoporous Nickel Cobalt Oxide Electrocatalyst for the Oxygen Evolution Reaction, *ACS Appl. Mater. Interfaces*, 2017, **9**(25), 21225–21233.

25 S. Cho, *et al.*, Optimizing nanosheet nickel cobalt oxide as an anode material for bifunctional electrochemical energy storage and oxygen electrocatalysis, *Electrochim. Acta*, 2018, **274**, 279–287.

26 Z. Li, *et al.*, Spinel $NiCo_2O_4$ 3-D nanoflowers supported on graphene nanosheets as efficient electrocatalyst for oxygen evolution reaction, *Int. J. Hydrogen Energy*, 2019, **44**(31), 16120–16131.

27 J. Wang, *et al.*, Hierarchical $NiCo_2O_4$ hollow nanospheres as high efficient bi-functional catalysts for oxygen reduction and evolution reactions, *Int. J. Hydrogen Energy*, 2016, **41**(21), 8847–8854.

28 X. Yin, *et al.*, 3D hierarchical network $NiCo_2S_4$ nanoflakes grown on Ni foam as efficient bifunctional electrocatalysts for both hydrogen and oxygen evolution reaction in alkaline solution, *Int. J. Hydrogen Energy*, 2017, **42**(40), 25267–25276.

29 Y. Gong, *et al.*, ACo_2O_4 (A = Ni, Zn, Mn) nanostructure arrays grown on nickel foam as efficient electrocatalysts for oxygen evolution reaction, *Int. J. Hydrogen Energy*, 2018, **43**(31), 14360–14368.

30 C. Zhu, *et al.*, Nickel cobalt oxide hollow nanosponges as advanced electrocatalysts for the oxygen evolution reaction, *Chem. Commun.*, 2015, **51**(37), 7851–7854.

31 C. F. Holder and R. E. Schaak, Tutorial on Powder X-ray Diffraction for Characterizing Nanoscale Materials, *ACS Nano*, 2019, **13**(7), 7359–7365.

32 C. F. Holder and R. E. Schaak, Tutorial on powder X-ray diffraction for characterizing nanoscale materials, *ACS Nano*, 2019, 7359–7365.

33 L. Huang, Porous $NiCo_2O_4$/C nanofibers replicated by cotton template as high-rate electrode materials for supercapacitors, *J. Materiomics.*, 2016, **2**(3), 248–255.

34 D. Chen, *et al.*, Experimental investigation of viscosity, enhanced thermal conductivity and zeta potential of a TiO_2 electrolyte-based nanofluid, *Int. Commun. Heat Mass Transfer*, 2020, **118**, 104840.

35 A. Ghasemi-Kahrizsangi, *et al.*, Effect of SDS modification of carbon black nanoparticles on corrosion protection behavior

23556 | *RSC Adv.*, 2023, **13**, 23547–23557

© 2023 The Author(s). Published by the Royal Society of Chemistry

of epoxy nanocomposite coatings, *Polym. Bull.*, 2015, **72**(9), 2297–2310.

36 E. Gileadi and E. Kirowa-Eisner, Some observations concerning the Tafel equation and its relevance to charge transfer in corrosion, *Corros. Sci.*, 2005, **47**(12), 3068–3085.

37 Y.-H. Fang and Z.-P. Liu, Tafel kinetics of electrocatalytic reactions: from experiment to first-principles, *ACS Catal.*, 2014, **4**(12), 4364–4376.

38 S. Anantharaj and S. Noda, Appropriate use of electrochemical impedance spectroscopy in water splitting electrocatalysis, *ChemElectroChem*, 2020, **7**(10), 2297–2308.

39 J. Masud, Cobalt selenide nanostructures: an efficient bifunctional catalyst with high current density at low coverage, *ACS Appl. Mater. Interfaces*, 2016, **8**(27), 17292–17302.

40 Y. Yang, NiCoO$_2$ nanowires grown on carbon fiber paper for highly efficient water oxidation, *Electrochim. Acta*, 2015, **174**, 246–253.

41 W. Ruan, Boosted electrocatalytic hydrogen production by methylene blue and urea and synergistic electrooxidation degradation, *Mater. Today Energy*, 2021, **22**, 100880.